High-spin structures in ^{155}Tb and signature splitting systematics of the $\pi h_{11/2}$ bands in odd $A \approx 160$ nuclei

D. J. Hartley,* T. B. Brown, F. G. Kondev, J. Pfohl, and M. A. Riley
Department of Physics, Florida State University, Tallahassee, Florida 32306

S. M. Fischer, R. V. F. Janssens, and D. T. Nisius
Argonne National Laboratory, Argonne, Illinois 60439

P. Fallon
Nuclear Science Division, Lawrence Berkeley National Laboratory, Berkeley, California 94720

W. C. Ma
Department of Physics, Mississippi State University, Starkville, Mississippi 39762

J. Simpson
CLRC, Daresbury Laboratory, Daresbury, Warrington, WA4 4AD, United Kingdom
(Received 22 June 1998)

The reactions ^{152}Sm(^{7}Li,4n) at 45 MeV and ^{124}Sn(^{36}S,$p4n$) at 165 MeV were used to study high-spin states of the $N=90$ nucleus ^{155}Tb. Previously known bands have been greatly extended in spin ($I \approx 45\hbar$) and a new decoupled sequence was identified. Several band crossings or quasiparticle alignments have been observed in each of the structures, and as a result a configuration assignment has been given to the new band. $B(M1)/B(E2)$ transition strength ratios have been extracted from the data and comparisons were made with theoretical predictions. A comprehensive analysis of the signature splitting in the energy levels and $B(M1)/B(E2)$ ratios for the $\pi h_{11/2}$ bands of the $A \approx 160$ region has been performed. Possible interpretations for the observed trends in the signature splitting of these structures are discussed. [S0556-2813(98)03211-7]

PACS number(s): 21.10.Re, 23.20.Lv, 27.70.+q

I. INTRODUCTION

The $N=90$ isotone chain is one of the most well studied groups of nuclei in the rare-earth region. Much of the interest lies in the fact that these nuclei dwell within a highly transitional area of deformation space. While the $N \leqslant 88$ nuclei are weakly deformed as a result of the $N=82$ shell gap, the $N \geqslant 92$ isotopes behave as well-deformed quantum rotors [1]. The intermediate deformations of the $N=90$ isotones permit these nuclei to be especially susceptible to shape driving forces by various competing processes. The manifestation of these forces has been observed at high-spin (band termination) and low-spin (signature splitting). In this work, we will report on new high-spin results for ^{155}Tb ($Z=65$), where angular momentum states have been populated in the same spin region ($I>40\hbar$) as band terminating states in nearby nuclei. The observation of the $\pi h_{11/2}$ band well beyond the first $i_{13/2}$ neutron crossing provides significant information pertaining to the signature splitting phenomenon in bands based on orbitals from this shell throughout the $A \approx 160$ region. Indeed, combining our recent observations of the $\pi h_{11/2}$ bands in ^{153}Tb [2], ^{155}Tb, ^{157}Tb [3], and ^{155}Eu [3] with previously published data from many odd-Z, odd-A nuclei has allowed a comprehensive study of the experimental signature splitting systematics of the $\pi h_{11/2}$ bands in the $A \approx 160$ region.

*Present address: Department of Physics and Astronomy, University of Tennessee, Knoxville, Tennessee 37996.

II. EXPERIMENTAL DETAILS AND RESULTS

Two complementary experiments have produced high-spin data on ^{155}Tb. One was performed at the Florida State University tandem-linac facility where the Florida State University array [4] was employed to collect the coincident γ rays. Three Compton-suppressed detectors were placed at 90° (with respect to the beam direction) and two other suppressed detectors were located at 145°. The reaction ^{152}Sm(^{7}Li,4n) was chosen with a beam energy of 45 MeV. The single foil target had a thickness of ~ 5 mg/cm^2, which was thick enough to stop the recoiling nuclei. Over 2×10^7 γ-γ events were recorded when two or more suppressed Ge detectors were in prompt coincidence ($\leqslant 100$ ns). The γ ray energies were calibrated using a ^{152}Eu source while the detector efficiencies were determined using both the singles data from the ^{152}Eu source and coincident data from the experimentally produced even-even nucleus ^{154}Gd [5]. The data were sorted into an $E_\gamma \times E_\gamma$ matrix which was inspected by the program ESCL8R [6]. The primary focus of this experiment was to produce clean data for identifying the multipolarity of transitions using the directional correlation from oriented states (DCO) method as well as determining the correct ordering of the transitions through the first $i_{13/2}$ neutron band crossing.

An experiment using the ^{36}S+^{124}Sn reaction was performed with the sulfur beam provided by the 88-Inch Cyclotron facility at the Lawrence Berkeley National Laboratory. The Gammasphere [7–9] spectrometer collected the coincidence events and was operated with 93 suppressed Ge

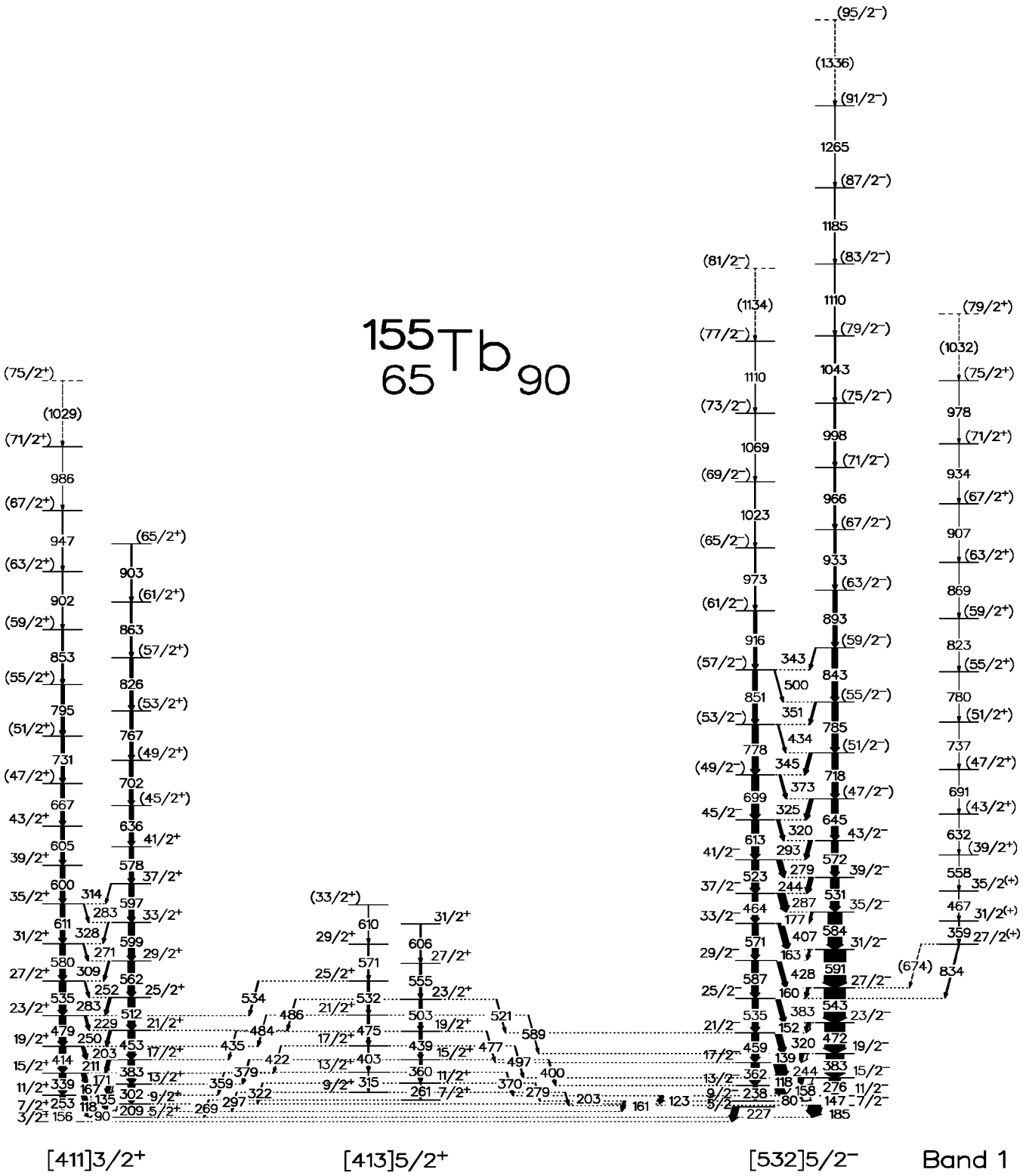

FIG. 1. The level scheme of ^{155}Tb derived from the present work. Tentative transitions or levels are denoted with broken lines.

detectors. Two thin stacked targets ($\sim$0.35 mg/cm^2) were used and a beam energy of 165 MeV was chosen for this experiment. The $4n$(^{156}Dy [10]), $5n$(^{155}Dy [11]), and $6n$(^{154}Dy [12]) neutron evaporation channels dominated the reaction cross section; however, a small percentage ($\sim$1–2 % of the total cross section) from the $p4n$ reaction channel leading to ^{155}Tb was observed. Due to the weakness of this $p4n$ channel, clean coincidence spectra were limited and thus the necessity for the ^{7}Li experiment to correctly identify the γ ray placement and ordering at low spins. Calibrations and efficiencies were determined with ^{152}Eu and ^{182}Ta sources. The coincident data were sorted into a $E_\gamma \times E_\gamma \times E_\gamma$ cube which was inspected by the program LEVIT8R [6].

The results from the two experiments are presented in both the level scheme of Fig. 1 and in Table I. Determination of spins and parities for new states was based upon previous

TABLE I. Results for ^{155}Tb.

E_x (keV) [a]	E_γ (keV) [b]	I_γ^{rel} [c]	I_γ^{rel} [d]	DCO ratios [e]	I_i^π [f]	I_f^π [f]
[411]3/2, $\alpha=+\frac{1}{2}$						
65.4	65.4 [g]					$\frac{5}{2}+\frac{3}{2}+$
274.2	208.8	24(1)	11(3)	1.03(6)	$\frac{9}{2}+$	$\frac{5}{2}+$
	118.3	69(4)	33(4)	0.90(5)	$\frac{9}{2}+$	$\frac{7}{2}+$
576.0	301.8	64(3)	32(4)	1.00(5)	$\frac{13}{2}+$	$\frac{9}{2}+$
	167.4	48(2)	21(2)	0.78(3)	$\frac{13}{2}+$	$\frac{11}{2}+$
958.9	382.9	61(3)	32(3)	1.02(3)	$\frac{17}{2}+$	$\frac{13}{2}+$
	211.4	26(1)	14(2)	0.76(4)	$\frac{17}{2}+$	$\frac{15}{2}+$
1411.5	452.6	48(2)	35(5)	0.99(3)	$\frac{21}{2}+$	$\frac{17}{2}+$
	249.8	14.5(6)	10(2)	0.70(3)	$\frac{21}{2}+$	$\frac{19}{2}+$
1923.6	512.1	33(2)	34(6)	0.95(3)	$\frac{25}{2}+$	$\frac{21}{2}+$
	282.8	7.2(3)	11(2)	0.69(3) [h]	$\frac{25}{2}+$	$\frac{23}{2}+$
2485.3	561.7	22(1)	32(6)	1.01(4)	$\frac{29}{2}+$	$\frac{25}{2}+$
	309.4	4.5(2)	7(2)	0.61(4)	$\frac{29}{2}+$	$\frac{27}{2}+$
3084.1	598.8	12.7(6)	28(8)	0.92(4)	$\frac{33}{2}+$	$\frac{29}{2}+$
	328.0	2.1(1)	<5	0.56(7)	$\frac{33}{2}+$	$\frac{31}{2}+$
3681.0	596.9	8.4(4)	24(8)	0.92(4)	$\frac{37}{2}+$	$\frac{33}{2}+$
	314.0	1.4(1)	<5		$\frac{37}{2}+$	$\frac{35}{2}+$
4259.4	578.4	2.7(1)	21(5)	1.2(1)	$\frac{41}{2}+$	$\frac{37}{2}+$
4895.2	635.8	<1	20(5)		$(\frac{45}{2}+)$	$\frac{41}{2}+$
5597	702 [i]		18(4)		$(\frac{49}{2}+)$	$(\frac{45}{2}+)$
6364	767 [i]		16(4)		$(\frac{53}{2}+)$	$(\frac{49}{2}+)$
7190	826 [i]		15(4)		$(\frac{57}{2}+)$	$(\frac{53}{2}+)$
8053	863 [i]		7(3)		$(\frac{61}{2}+)$	$(\frac{57}{2}+)$
8956	903 [i]		<5		$(\frac{65}{2}+)$	$(\frac{61}{2}+)$
[411]3/2, $\alpha=-\frac{1}{2}$						
155.8	155.8	$\sim$15			$\frac{7}{2}+$	$\frac{3}{2}+$
	90.3 [g]				$\frac{7}{2}+$	$\frac{5}{2}+$
408.6	252.8	38(3)	27(5)	0.98(3)	$\frac{11}{2}+$	$\frac{7}{2}+$
	134.5	60(3)	24(3)	0.85(5)	$\frac{11}{2}+$	$\frac{9}{2}+$
747.4	338.8	69(3)	34(3)	1.04(2)	$\frac{15}{2}+$	$\frac{11}{2}+$
	171.4	32(1)	14(2)	0.73(2)	$\frac{15}{2}+$	$\frac{13}{2}+$
1161.4	414.0	62(3)	36(8)	1.04(2)	$\frac{19}{2}+$	$\frac{15}{2}+$
	202.6	17.6(8)	11(2)	0.68(4)	$\frac{19}{2}+$	$\frac{17}{2}+$
1640.7	479.3	51(2)	35(7)	1.00(2)	$\frac{23}{2}+$	$\frac{19}{2}+$
	229.1	9.9(5)	7(2)	0.70(3)	$\frac{23}{2}+$	$\frac{21}{2}+$
2175.7	535.0	34(2)	34(5)	0.96(3)	$\frac{27}{2}+$	$\frac{23}{2}+$
	252.2	5.7(3)	<5		$\frac{27}{2}+$	$\frac{25}{2}+$
2756.1	580.4	18.5(8)	28(6)	0.98(5)	$\frac{31}{2}+$	$\frac{27}{2}+$
	270.7	2.3(1)	<5	0.53(5)	$\frac{31}{2}+$	$\frac{29}{2}+$
3367.2	611.1	10.4(4)	26(5)	1.02(6)	$\frac{35}{2}+$	$\frac{31}{2}+$
	283.1	1.3(1)	<5	0.53(4) [h]	$\frac{35}{2}+$	$\frac{33}{2}+$
3966.7	599.5	4.5(2)	24(6)	0.90(7)	$\frac{39}{2}+$	$\frac{35}{2}+$
4572.1	605.4	2.8(1)	21(4)	0.9(1)	$\frac{43}{2}+$	$\frac{39}{2}+$
5238.7	666.6	<1	19(4)		$(\frac{47}{2}+)$	$\frac{43}{2}+$
5970	731 [i]		17(4)		$(\frac{51}{2}+)$	$(\frac{47}{2}+)$
6765	795 [i]		16(4)		$(\frac{55}{2}+)$	$(\frac{51}{2}+)$
7618	853 [i]		8(3)		$(\frac{59}{2}+)$	$(\frac{55}{2}+)$
8520	902 [i]		<5		$(\frac{63}{2}+)$	$(\frac{59}{2}+)$
9467	947 [i]		<5		$(\frac{67}{2}+)$	$(\frac{63}{2}+)$
10453	986 [i]		<5		$(\frac{71}{2}+)$	$(\frac{67}{2}+)$

TABLE I. (*Continued*).

E_x (keV) [a]	E_γ (keV) [b]	I_γ^{rel} [c]	I_γ^{rel} [d]	DCO ratios [e]	I_i^π [f]	I_f^π [f]
(11482)	(1029 [i])		<5		$(\frac{75}{2}^+)$	$(\frac{71}{2}^+)$
[532]5/2, $\alpha=+\frac{1}{2}$						
227.0	227.0	$\sim$65		0.69(2)	$\frac{5}{2}^-$	$\frac{3}{2}^+$
317.0	66.9 [g]				$\frac{9}{2}^-$	$\frac{7}{2}^-$
	161.3	$\sim$20			$\frac{9}{2}^-$	$\frac{7}{2}^+$
555.2	238.2	35(2)	21(2)	1.06(4)	$\frac{13}{2}^-$	$\frac{9}{2}^-$
	157.9	81(4)	45(5)	0.85(3)	$\frac{13}{2}^-$	$\frac{11}{2}^-$
916.9	361.7	48(2)	40(6)	0.99(4)	$\frac{17}{2}^-$	$\frac{13}{2}^-$
	243.8	54(2)	47(4)	0.81(2) [h]	$\frac{17}{2}^-$	$\frac{15}{2}^-$
1376.3	459.4	44(2)	38(4)	1.02(4)	$\frac{21}{2}^-$	$\frac{17}{2}^-$
	320.0	29(1)	27(3)	0.78(4)	$\frac{21}{2}^-$	$\frac{19}{2}^-$
1911.4	535.1	32(1)	33(3)	1.02(4)	$\frac{25}{2}^-$	$\frac{21}{2}^-$
	383.1	22(1)	19(2)	0.88(5) [h]	$\frac{25}{2}^-$	$\frac{23}{2}^-$
2498.8	587.4	16.8(8)	34(6)	0.9(1)	$\frac{29}{2}^-$	$\frac{25}{2}^-$
	427.6	9.5(5)	18(3)	0.74(4)	$\frac{29}{2}^-$	$\frac{27}{2}^-$
3069.6	570.8	10.8(5)	32(3)	1.04(7)	$\frac{33}{2}^-$	$\frac{29}{2}^-$
	407.1	8.7(4)	27(4)	0.75(3)	$\frac{33}{2}^-$	$\frac{31}{2}^-$
3533.3	463.7	7.5(4)	30(6)	0.99(9)	$\frac{37}{2}^-$	$\frac{33}{2}^-$
	286.5	6.9(3)	31(3)	0.59(2)	$\frac{37}{2}^-$	$\frac{35}{2}^-$
4056.6	523.3	4.6(2)	36(5)	1.0(1)	$\frac{41}{2}^-$	$\frac{37}{2}^-$
	279.1	2.4(1)	21(2)	0.63(4)	$\frac{41}{2}^-$	$\frac{39}{2}^-$
4669.5	612.9	3.2(1)	37(6)	0.9(2)	$\frac{45}{2}^-$	$\frac{41}{2}^-$
	320.0	1.0(1)	11(2)		$\frac{45}{2}^-$	$\frac{43}{2}^-$
5368.0	698.5	<1	37(8)		$(\frac{49}{2}^-)$	$\frac{45}{2}^-$
	373 [i]		8(2)		$(\frac{49}{2}^-)$	$(\frac{47}{2}^-)$
6146	778 [i]		33(4)		$(\frac{53}{2}^-)$	$(\frac{49}{2}^-)$
	434 [i]		<5		$(\frac{53}{2}^-)$	$(\frac{51}{2}^-)$
6997	851 [i]		24(4)		$(\frac{57}{2}^-)$	$(\frac{53}{2}^-)$
	500 [i]		<5		$(\frac{57}{2}^-)$	$(\frac{55}{2}^-)$
7913	916 [i]		17(3)		$(\frac{61}{2}^-)$	$(\frac{57}{2}^-)$
8886	973 [i]		7(2)		$(\frac{65}{2}^-)$	$(\frac{61}{2}^-)$
9909	1023 [i]		<5		$(\frac{69}{2}^-)$	$(\frac{65}{2}^-)$
10978	1069 [i]		<5		$(\frac{73}{2}^-)$	$(\frac{69}{2}^-)$
12088	1110 [i]		<5		$(\frac{77}{2}^-)$	$(\frac{73}{2}^-)$
(13222)	(1134 [i])		<5		$(\frac{81}{2}^-)$	$(\frac{77}{2}^-)$
[532]5/2, $\alpha=-\frac{1}{2}$						
250.0	184.6	$\sim$165		0.64(1)	$\frac{7}{2}^-$	$\frac{5}{2}^+$
397.4	147.4	$\sim$10			$\frac{11}{2}^-$	$\frac{7}{2}^-$
	80.4 [g]				$\frac{11}{2}^-$	$\frac{9}{2}^-$
	123.3	$\sim$1			$\frac{11}{2}^-$	$\frac{9}{2}^+$
673.0	275.6	71(3)	53(5)	1.02(3)	$\frac{15}{2}^-$	$\frac{11}{2}^-$
	118.0	47(2)	32(4)	0.85(5)	$\frac{15}{2}^-$	$\frac{13}{2}^-$
1056.3	383.3	116(5)	88(6)	1.01(3)	$\frac{19}{2}^-$	$\frac{15}{2}^-$
	139.4	25(1)	22(3)	0.70(4)	$\frac{19}{2}^-$	$\frac{17}{2}^-$
1528.2	471.9	100	100	1.02(2)	$\frac{23}{2}^-$	$\frac{19}{2}^-$
	151.9	9.6(5)	12(2)	0.73(4)	$\frac{23}{2}^-$	$\frac{21}{2}^-$
2071.0	542.8	74(3)	105(8)	1.02(2)	$\frac{27}{2}^-$	$\frac{23}{2}^-$
	159.7	4.8(3)	7(1)	0.53(5) [h]	$\frac{27}{2}^-$	$\frac{25}{2}^-$
2662.3	591.3	43(2)	108(9)	1.03(3)	$\frac{31}{2}^-$	$\frac{27}{2}^-$
	163.3	2.4(2)	6(1)	0.62(8)	$\frac{31}{2}^-$	$\frac{29}{2}^-$

TABLE I. (*Continued*).

E_x (keV) [a]	E_γ (keV) [b]	I_γ^{rel} [c]	I_γ^{rel} [d]	DCO ratios [e]	I_i^π [f]	I_f^π [f]
3246.6	584.3	19.3(9)	70(7)	1.02(3)	$\frac{35}{2}^-$	$\frac{31}{2}^-$
	177.2	1.5(1)	7(1)	0.62(8)	$\frac{35}{2}^-$	$\frac{33}{2}^-$
3777.5	530.9	7.2(4)	41(4)	1.04(5)	$\frac{39}{2}^-$	$\frac{35}{2}^-$
	244.0	2.4(2)	18(2)	0.75(2) [h]	$\frac{39}{2}^-$	$\frac{37}{2}^-$
4349.8	572.3	3.6(2)	32(4)	1.07(5)	$\frac{43}{2}^-$	$\frac{39}{2}^-$
	293.2	1.4(1)	17(2)	0.7(1)	$\frac{43}{2}^-$	$\frac{41}{2}^-$
4995.2	645.4	<1	32(4)		$(\frac{47}{2}^-)$	$\frac{43}{2}^-$
	(325.4)	<1	17(2)		$(\frac{47}{2}^-)$	$\frac{45}{2}^-$
5713	718 [i]		31(5)		$(\frac{51}{2}^-)$	$(\frac{47}{2}^-)$
	345 [i]		14(3)		$(\frac{51}{2}^-)$	$(\frac{49}{2}^-)$
6498	785 [i]		31(4)		$(\frac{55}{2}^-)$	$(\frac{51}{2}^-)$
	351 [i]		8(3)		$(\frac{55}{2}^-)$	$(\frac{53}{2}^-)$
7341	843 [i]		27(4)		$(\frac{59}{2}^-)$	$(\frac{55}{2}^-)$
	343 [i]		5(2)		$(\frac{59}{2}^-)$	$(\frac{57}{2}^-)$
8234	893 [i]		21(3)		$(\frac{63}{2}^-)$	$(\frac{59}{2}^-)$
9167	933 [i]		10(3)		$(\frac{67}{2}^-)$	$(\frac{63}{2}^-)$
10133	966 [i]		8(2)		$(\frac{71}{2}^-)$	$(\frac{67}{2}^-)$
11131	998 [i]		7(1)		$(\frac{75}{2}^-)$	$(\frac{71}{2}^-)$
12174	1043 [i]		<5		$(\frac{79}{2}^-)$	$(\frac{75}{2}^-)$
13284	1110 [i]		<5		$(\frac{83}{2}^-)$	$(\frac{79}{2}^-)$
14469	1185 [i]		<5		$(\frac{87}{2}^-)$	$(\frac{83}{2}^-)$
15734	1265 [i]		<5		$(\frac{91}{2}^-)$	$(\frac{87}{2}^-)$
(17070)	(1336 [i])		<5		$(\frac{95}{2}^-)$	$(\frac{91}{2}^-)$
[413]5/2, $\alpha=+\frac{1}{2}$						
452.6	296.7	1.7(1)		0.46(6)	$\frac{9}{2}^+$	$\frac{7}{2}^+$
	202.6	2.7(2)		0.56(6)	$\frac{9}{2}^+$	$\frac{7}{2}^-$
767.2	314.6	3.4(2)		1.02(7)	$\frac{13}{2}^+$	$\frac{9}{2}^+$
	358.5	2.1(1)		0.51(5)	$\frac{13}{2}^+$	$\frac{11}{2}^+$
	369.7	2.2(1)		0.64(6)	$\frac{13}{2}^+$	$\frac{11}{2}^-$
1170.6	403.4	8.0(4)		0.88(8)	$\frac{17}{2}^+$	$\frac{13}{2}^+$
	422.3	2.1(1)			$\frac{17}{2}^+$	$\frac{15}{2}^+$
	497.4	2.9(2)			$\frac{17}{2}^+$	$\frac{15}{2}^-$
1645.7	475.1	10.2(5)		1.07(9)	$\frac{21}{2}^+$	$\frac{17}{2}^+$
	484.1	2.1(1)			$\frac{21}{2}^+$	$\frac{19}{2}^+$
	589.2	2.1(2)			$\frac{21}{2}^+$	$\frac{19}{2}^-$
2178.1	532.4	10.8(6)		0.85(6)	$\frac{25}{2}^+$	$\frac{21}{2}^+$
	534.2	2.4(3)			$\frac{25}{2}^+$	$\frac{23}{2}^+$
2749.5	571.4	6.1(3)		1.05(9)	$\frac{29}{2}^+$	$\frac{25}{2}^+$
3359.2	609.7	2.0(1)			$(\frac{33}{2}^+)$	$\frac{29}{2}^+$
[413]5/2, $\alpha=-\frac{1}{2}$						
335.0	269.4	3.0(2)			$\frac{7}{2}^+$	$\frac{5}{2}^+$
595.9	260.9	2.3(1)		1.1(1)	$\frac{11}{2}^+$	$\frac{7}{2}^+$
	321.6	3.0(2)		0.59(7)	$\frac{11}{2}^+$	$\frac{9}{2}^+$
	278.7	3.6(3)		0.46(5)	$\frac{11}{2}^+$	$\frac{9}{2}^-$
955.4	359.5	9.7(5)		1.02(6)	$\frac{15}{2}^+$	$\frac{11}{2}^+$
	379.4	3.2(3)		0.39(5)	$\frac{15}{2}^+$	$\frac{13}{2}^+$
	400.1	4.0(2)		0.49(5)	$\frac{15}{2}^+$	$\frac{13}{2}^-$
1394.1	438.7	12.0(6)		0.91(7)	$\frac{19}{2}^+$	$\frac{15}{2}^+$
	435.3	1.8(1)			$\frac{19}{2}^+$	$\frac{17}{2}^+$
	477.2	3.8(3)			$\frac{19}{2}^+$	$\frac{17}{2}^-$

TABLE I. (*Continued*).

E_x (keV) [a]	E_γ (keV) [b]	I_γ^{rel} [c]	I_γ^{rel} [d]	DCO ratios [e]	I_i^π [f]	I_f^π [f]
1897.4	503.3	11.8(6)		1.08(7)	$\frac{23}{2}^+$	$\frac{19}{2}^+$
	485.9	1.6(1)			$\frac{23}{2}^+$	$\frac{21}{2}^+$
	520.9	2.2(1)			$\frac{23}{2}^+$	$\frac{21}{2}^-$
2452.8	555.4	9.8(5)		1.02(6)	$\frac{27}{2}^+$	$\frac{23}{2}^+$
3058.4	605.6	4.8(3)		0.96(8)	$\frac{31}{2}^+$	$\frac{27}{2}^+$
Band 1, $\alpha=-\frac{1}{2}$						
2745.2	833.8	6.0(3)	9(3)	0.58(6)	$\frac{27}{2}(+)$	$\frac{25}{2}^-$
	(674.0)	<1			$\frac{27}{2}(+)$	$\frac{27}{2}^-$
3104.5	359.3	3.9(2)	8(3)	1.2(2)	$\frac{31}{2}(+)$	$\frac{27}{2}(+)$
3571.7	467.2	2.8(2)	8(3)	1.1(2)	$\frac{35}{2}(+)$	$\frac{31}{2}(+)$
4130.1	558.4	1.0(1)	7(2)		$(\frac{39}{2}^+)$	$\frac{35}{2}(+)$
4762.1	632.0	<1	7(2)		$(\frac{43}{2}^+)$	$(\frac{39}{2}^+)$
5453	691 [i]		6(2)		$(\frac{47}{2}^+)$	$(\frac{43}{2}^+)$
6190	737 [i]		6(2)		$(\frac{51}{2}^+)$	$(\frac{47}{2}^+)$
6970	780 [i]		5(1)		$(\frac{55}{2}^+)$	$(\frac{51}{2}^+)$
7793	823 [i]		<5		$(\frac{59}{2}^+)$	$(\frac{55}{2}^+)$
8662	869 [i]		<5		$(\frac{63}{2}^+)$	$(\frac{59}{2}^+)$
9569	907 [i]		<5		$(\frac{67}{2}^+)$	$(\frac{63}{2}^+)$
10503	934 [i]		<5		$(\frac{71}{2}^+)$	$(\frac{67}{2}^+)$
11481	978 [i]		<5		$(\frac{75}{2}^+)$	$(\frac{71}{2}^+)$
(12513)	(1032 [i])		<5		$(\frac{79}{2}^+)$	$(\frac{75}{2}^+)$

[a]Level energies; band-head excitation energies have been taken from previous work [13,14] except for band 1.

[b]Energies determined from the ^{152}Sm(^{7}Li,4n) reaction unless otherwise noted. Accurate to 0.2 keV for most transitions. For weak or contaminated transitions, accurate to 0.5 keV.

[c]Relative γ-ray intensities [$I_\gamma(471.9)\equiv 100$] measured from the ^{152}Sm(^{7}Li,4n) reaction.

[d]Relative γ-ray intensities [$I_\gamma(471.9)\equiv 100$] measured from the ^{124}Sn(^{36}S,$p4n$) reaction.

[e]DCO ratios were determined by using a sum of one or more stretched $E2$ transitions as gates. DCO ratios were measured using the ^{152}Sm(^{7}Li,4n) reaction.

[f]Spin and parity assignments are based on the previous work [13,14] and on the DCO ratio determining the multipolarity of any new transition.

[g]Transition observed previously, but not in the present experimental work.

[h]DCO value has been contaminated by an unresolvable doublet of different multipolarity or mixing ratio.

[i]Energy determined from the ^{124}Sn(^{36}S,$p4n$) reaction. Accurate to 1 keV.

work [13,14] and DCO measurements from the ^{7}Li experiment. The DCO ratios were calculated by the expression

$$R_{\text{DCO}}=\frac{I_{\gamma_1}(\text{at } 145^\circ;\ \text{in coincidence with } \gamma_2 \text{ at } 90^\circ)}{I_{\gamma_1}(\text{at } 90^\circ;\ \text{in coincidence with } \gamma_2 \text{ at } 145^\circ)},$$

where γ_2 is normally a stretched $E2(\Delta I=2)$ transition. For averaging purposes and greater statistics, a summed coincidence spectrum from several successive $E2$ transitions was used whenever possible. Spin and parity assignments have been put in parentheses in Fig. 1 if reliable DCO values were not attainable. Tentative transitions or levels are denoted by dashed lines in the level scheme.

Previous high-spin studies of ^{155}Tb [13,14] established rotational bands based on the [411]3/2, [532]5/2, and [413]5/2 proton states up to $I^\pi=\frac{23}{2}^+$, $\frac{23}{2}^-$, and $\frac{13}{2}^+$, respectively. We used a similar ^{124}Sn(^{36}S,$p4n$) reaction with Gammasphere in its early implementation phase and established the [532]5/2 band up to spin $(\frac{67}{2}^-)$ in Ref. [15]. The combination of our experiments presented in this work has extended the [411]3/2, [532]5/2, and [413]5/2 bands to spin $(\frac{75}{2}^+)$,$(\frac{95}{2}^-)$, and $(\frac{33}{2}^+)$, respectively. We have also discovered a new decoupled band, labeled band 1 in Fig. 1, observed to spin $(\frac{79}{2}^+)$. Including our earlier work [15], over 115 new transitions and 80 new levels have been identified in ^{155}Tb. For further discussion about the individual bands, the excitation energy of the levels (minus a rigid rotor) and the relative γ ray intensities have been plotted versus spin in Figs. 2(a) and 2(b), respectively. In Fig. 2(b), the intensities from both the ^{7}Li (solid lines with symbols) and ^{36}S (dashed lines without symbols) experiments have been plotted.

Although the [411]3/2 band is the ground-state band of ^{155}Tb, it only remains yrast up to $I=\frac{9}{2}$ [Fig. 2(a)] where the $\alpha=-\frac{1}{2}$ signature of the [532]5/2 band becomes yrast. A

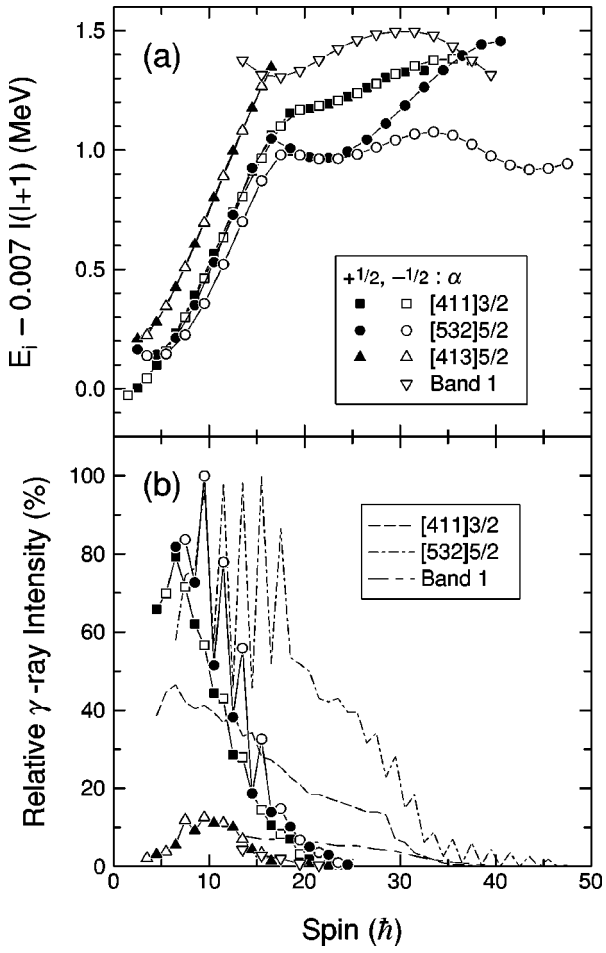

FIG. 2. (a) Excitation energy of the angular momentum states (minus a rigid rotor) versus spin for the four observed bands in ^{155}Tb. (b) Relative γ-ray intensities of the bands versus spin. The solid lines with symbols denote values from the ^{7}Li experiment, whereas the dashed lines without symbols are from the ^{36}S experiment.

coincidence spectrum for this band is given in Fig. 3(a) where lower spin ($I<\frac{43}{2}$) transitions are shown from the ^{7}Li experiment and the higher spin ($I>\frac{43}{2}$) transitions from the ^{36}S experiment are displayed in the high-energy insert. While the $\alpha=-\frac{1}{2}$ signature was extended to $I=(\frac{75}{2})$, the $\alpha=+\frac{1}{2}$ signature could only be observed up to $I=(\frac{65}{2})$, see Fig. 1. This was due to a lack of clean coincidence gates near the top of the $\alpha=+\frac{1}{2}$ signature. An 872 keV transition [marked with a star in the insert of Fig. 3(a)] also showed evidence that it was in coincidence with the $\alpha=+\frac{1}{2}$ signature; however, it could not be firmly placed in the level scheme.

Figure 3(b) displays a coincidence spectrum for the [532]5/2 band in a similar manner as Fig. 3(a). As stated previously, the $\alpha=-\frac{1}{2}$ signature quickly becomes yrast and, as can be seen in Fig. 2(a), remains yrast throughout the observed spin region. Figure 2(a) also indicates that the $\alpha=-\frac{1}{2}$ signature (open circles) is favored over the $\alpha=+\frac{1}{2}$ signature (solid circles) in the spin region $I<\frac{39}{2}$. This explains the staggering seen in the intensity profile of Fig. 2(b) for the [532]5/2 band as the favored states will be more intensely populated by the nucleus. However, from $\frac{39}{2}<I<(\frac{51}{2})$, both signatures are equally favored [Fig. 2(a)]; thus the intensity profile becomes dramatically smoother. The intensity staggering reappears at $I>(\frac{51}{2})$ in Fig. 2(b) as the $\alpha=-\frac{1}{2}$ signature becomes strongly favored again. The $\alpha=+\frac{1}{2}$ signature could only be extended to $I=(\frac{81}{2})$ since it is located at much higher excitation energy than the $\alpha=-\frac{1}{2}$ signature at high-spin.

The [413]5/2 band was the only structure observed in the ^{7}Li experiment exclusively. A coincidence spectrum for this band has been provided in Fig. 4(a). Although the intraband $\Delta I=1$ transitions were not observed, one can see by both Figs. 2(a) and 2(b) that the two rotational structures act as signature partners. The $B(M1)/B(E2)$ ratios of the [413]5/2 band in ^{157}Tb [3] were very low ($<0.1\ \mu_N/e\mathrm{b}$), thus the $\Delta I=1$ transitions were expected to be weak. One may notice from Fig. 1 that the [413]5/2 band feeds both the [411]3/2 band, which will be discussed later, and the [532]5/2 band. The decay into the latter, opposite-parity band is also observed in ^{157}Tb. As described in Refs. [3,16–18], the enhanced $E1$ transitions are likely a result of large contributions to the $\mathcal{M}(E1)$ matrix element from the even-even core.

The decoupled rotational sequence labeled band 1 in Fig. 1 was initially observed in the ^{7}Li experiment up to spin $(\frac{43}{2})$. The coincidence spectrum given in Fig. 4(b) shows how band 1 was extended to spin $(\frac{79}{2})$ in the ^{36}S experiment. The band primarily feeds the $I=\frac{25}{2}$ state in the [532]5/2 band through the 833.8 keV transition (see Fig. 1). DCO analysis on this γ ray revealed a ratio of $R_{\mathrm{DCO}}=0.58(6)$, thus confirming it as a $\Delta I=1$ transition. With the lowest observed state at 2745.2 keV and spin $I=\frac{27}{2}$, band 1 appears to be a candidate for a three-quasiparticle band which likely involves an $h_{11/2}$ proton since it decays into the [532]5/2 band. Band 1 strongly resembles a decoupled structure found in ^{153}Tb [2], which was assigned positive-parity; therefore, we have also tentatively assigned the same parity to band 1.

III. ALIGNMENTS AND BAND CROSSINGS

The rotational alignments of the bands in ^{155}Tb are presented in Figs. 5(a) and 5(b). For clarity, the bands based on positive-parity orbitals and those with a $h_{11/2}$ proton in their initial configuration have been separated into panels (a) and (b), respectively. The Harris parametrization [19] was employed with $\mathcal{J}_0=32\hbar^2/\mathrm{MeV}$ and $\mathcal{J}_1=34\hbar^4/\mathrm{MeV}^3$. These commonly used parameters were chosen such that the correct reference is subtracted in the three-quasiparticle region (above the $i_{13/2}$ neutron crossing). In order to simplify the following discussion, the quasiparticle orbitals have been labeled in the usual alphabetic manner [20–22]. The quasineutron orbitals are labeled with respect to parity and signature $(\pi,\alpha)_n$ as

$$\mathrm{A}=\left(+,+\frac{1}{2}\right)_1,\quad \mathrm{C}=\left(+,+\frac{1}{2}\right)_2,\quad \mathrm{E}=\left(-,+\frac{1}{2}\right)_2,$$

$$\mathrm{B}=\left(+,-\frac{1}{2}\right)_1,\quad \mathrm{D}=\left(+,-\frac{1}{2}\right)_2,\quad \mathrm{F}=\left(-,-\frac{1}{2}\right)_1.$$

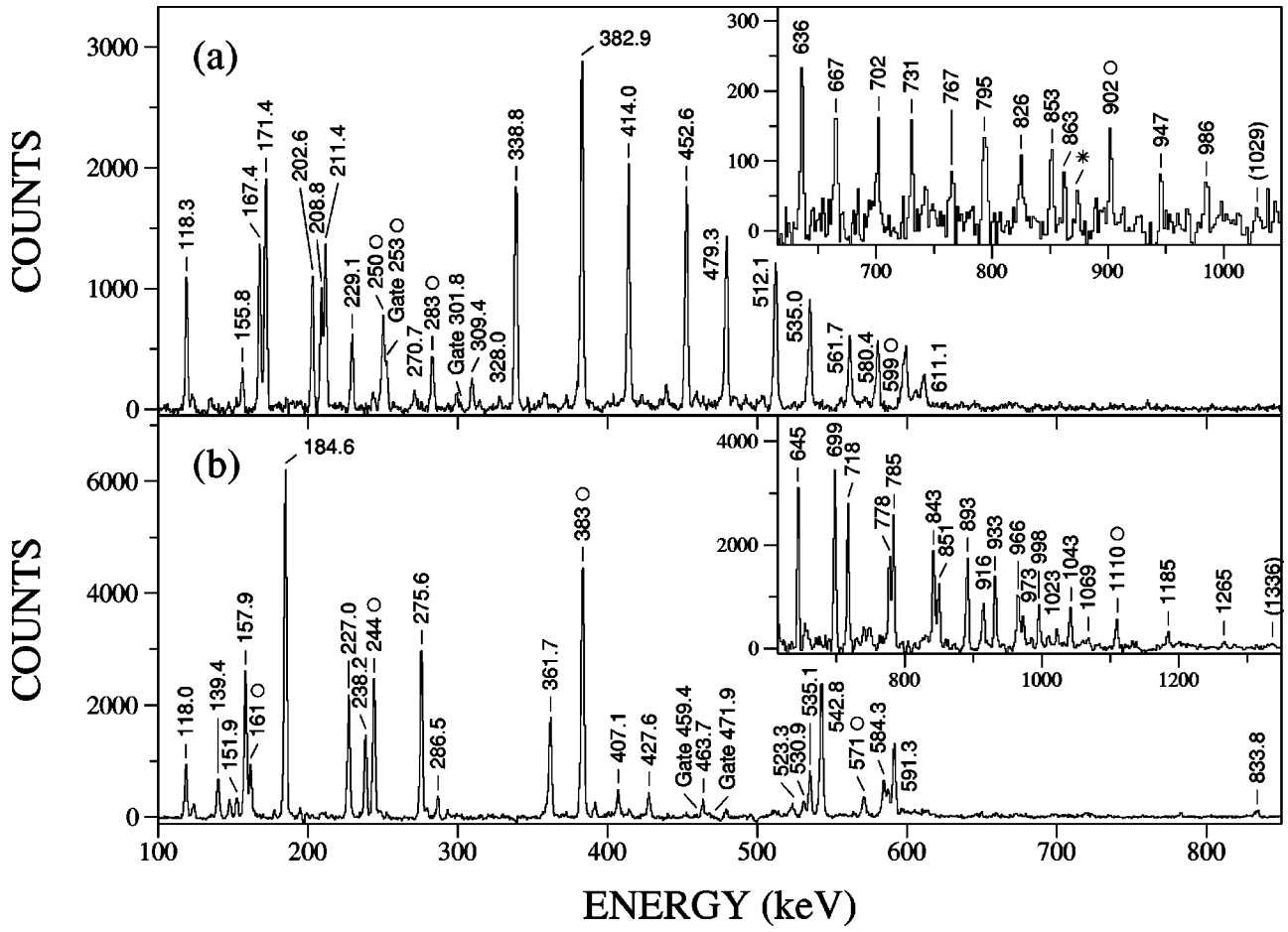

FIG. 3. (a) Spectrum of the [411]3/2 band from transitions in coincidence with the 252.8 and 301.8 keV γ rays in the ^{7}Li experiment. The high-energy inset is the result of summing many coincidence spectra from the ^{36}S experiment. (b) Spectrum of the [532]5/2 band from transitions in coincidence with the 459.4 and 471.9 keV γ rays in the ^{7}Li experiment. Once again the high-energy inset is a result of summing many coincidence spectra from the ^{36}S experiment. An open circle denotes that the transition is at least a doublet and, therefore, an exact energy is not labeled.

The subscript n numbers the quasiparticles' excitations of a specific signature and parity starting with the lowest in energy. The quasiproton orbitals are labeled as

$$\mathrm{A}_p=\left(-,-\frac{1}{2}\right)_1, \quad \mathrm{B}_p=\left(-,+\frac{1}{2}\right)_1,$$

$$\mathrm{C}_p=\left(-,-\frac{1}{2}\right)_2, \quad \mathrm{D}_p=\left(-,+\frac{1}{2}\right)_2,$$

$$\mathrm{E}_p=\left(+,+\frac{1}{2}\right)_1, \quad \mathrm{F}_p=\left(+,-\frac{1}{2}\right)_1.$$

The A, B, C, and D orbitals are associated with the $i_{13/2}$ shell, while E, F are a mixture of orbitals from the $h_{9/2}$ and $f_{7/2}$ shells. The A_p, B_p, C_p, and D_p orbitals are associated with the $h_{11/2}$ shell and the E_p, F_p orbitals are from the $d_{5/2}$ shell. Cranked shell model calculations were performed to help identify the nature of observed crossings. However, since many similar quasiparticle diagrams relevant for discussing band crossings in ^{155}Tb and neighboring nuclei have been published, for example see Refs. [5,22–24], these diagrams are not repeated here.

The alignment plot for the [411]3/2 band in Fig. 5(a) indicates that two crossings are observed. The AB crossing occurs at a rotational frequency of $\hbar\omega_c \approx 0.30$ MeV and is associated with a pair of low-K $i_{13/2}$ neutrons aligning their spin with the rotation axis. An alignment gain of $\Delta i = 9.8\hbar$ is observed, which is a typical amount for this crossing [22]. One may note the difference in the AB crossing for the [411]3/2 and [532]5/2 [Fig. 5(b)] bands. While a slight backbend is seen in the [532]5/2 band, only an upbend is observed in the [411]3/2 band. This indicates a larger interaction strength in the [411]3/2 band, which may suggest that this band has slightly higher deformation [22] than the [532]5/2 band which is similar to that observed in ^{157}Tb [3]. The alignment gain in the second crossing ($\Delta i \geqslant 5\hbar$) is significantly more gradual than the AB crossing. For this reason, it is difficult to accurately identify the crossing frequency; however, it appears to be approximately 0.44 MeV. The lowest proton crossing $\mathrm{A}_p\mathrm{B}_p$ has been identified in $^{157}_{67}$Ho [25], $^{159}_{69}$Tm [26], $^{161}_{71}$Lu [27], $^{163}_{71}$Lu [28], and neighboring even-even nuclei (see Ref. [23], and references therein) with crossing frequencies and alignment gains similar to those observed in ^{155}Tb. The gradual gain in alignment may be associated with a strong interaction between the three and five-quasiparticle bands [22] and is very similar to the

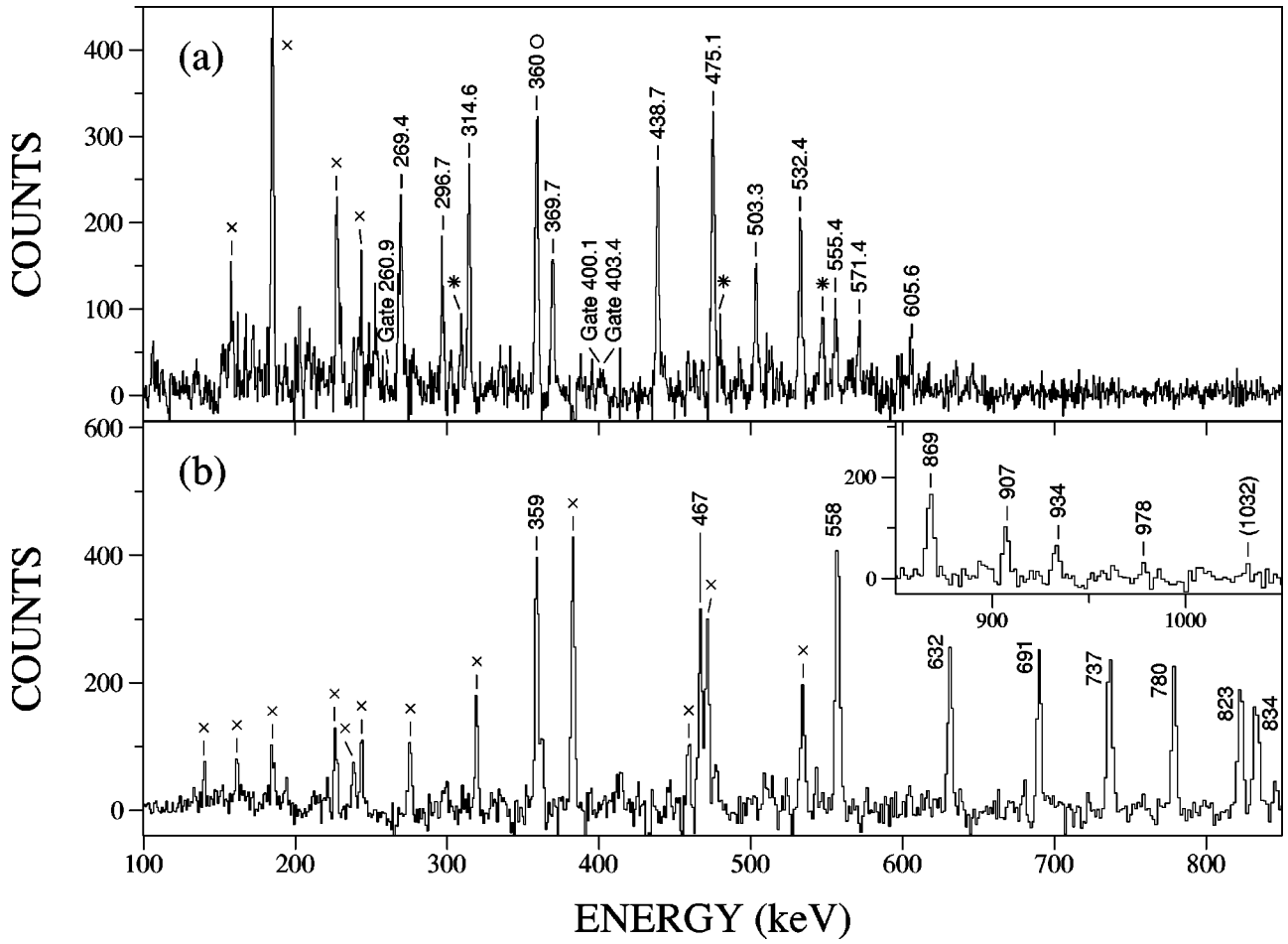

FIG. 4. (a) Spectrum of the [413]5/2 band from transitions in coincidence with the 260.9, 400.1, and 403.4 keV γ rays in the ^{7}Li experiment. (b) Spectrum of band 1 resulting from a sum of many coincidence spectra in the ^{36}S experiment. The high-energy inset is the continuation of band 1 from the same spectrum. The crosses in panels (a) and (b) denote transitions from the [532]5/2 band while an open circle once again denotes the transition is at least a doublet such that an exact energy is not labeled. Peaks marked with an asterisk are contaminent transitions.

A_pB_p crossing in ^{157}Ho. The band crossing frequencies and alignment gains observed in the ^{155}Tb bands have been summarized in Table II.

One may notice that the $\alpha=+\frac{1}{2}$ signature (solid squares) of the [411]3/2 band begins to differentiate itself from the $\alpha=-\frac{1}{2}$ signature at $\hbar\omega>0.4$ MeV, see Fig. 5(a). An unobserved band could be perturbing the states in the $\alpha=+\frac{1}{2}$ signature to cause this variance. The 872 keV transition mentioned in Sec. II may well be a link to this structure.

The alignment of the [413]5/2 band [Fig. 5(a)] resembles the [411]3/2 band over a frequency range of $\hbar\omega\approx0.05$ to 0.25 MeV. The same scenario is observed between these two bands in ^{157}Tb [3] where we attributed this occurrence to the fact that the bands are pseudospin partners. In the pseudospin scheme both bands have identical Nilsson values $[\tilde{N},\tilde{n}_z,\tilde{\Lambda}]$ but differ in $\tilde{\Omega}$ $(\tilde{\Omega}=\tilde{\Lambda}\pm\frac{1}{2})$ [29]. Thus, it is not surprising to observe the similar alignment profile at low frequency ($\hbar\omega<0.25$ MeV) between these bands, which come from the same pseudospin orbital. This is also the likely cause of the strong coupling between the bands as seen in Fig. 1. Unfortunately, the [413]5/2 band in ^{155}Tb could not be extended past the AB crossing to observe if this trend continues into the three-quasiparticle region.

The alignment of the [532]5/2 band is displayed in Fig. 5(b). Both signatures experience a slight backbend in the AB crossing at $\hbar\omega_c=0.280$ and 0.269 MeV for the $\alpha=+\frac{1}{2}$ and $\alpha=-\frac{1}{2}$ signatures, respectively. An alignment gain of $\Delta i=9.3\hbar$ was also observed in each signature. Another crossing occurs at $\hbar\omega_c\approx0.47$ MeV with an alignment gain of $\Delta i=5.8\hbar$ in the $\alpha=-\frac{1}{2}$ signature. Since the $\alpha=+\frac{1}{2}$ passes through this crossing region, we associate the crossing with the alignment of the B_p and C_p protons. This assignment is consistent with the B_pC_p crossings observed in ^{157}Ho [25] and ^{159}Tm [26], where the corresponding crossing frequencies are 0.48 and 0.46 MeV, respectively. An interesting feature of the $\alpha=-\frac{1}{2}$ signature in ^{155}Tb is that, unlike in ^{157}Ho and possibly ^{159}Tm, there are no signs of band termination effects up to the observed $I=(\frac{95}{2})$ state. A similar difference is observed between ^{156}Dy and ^{158}Er where effects of band termination are seen at higher spin in the former nucleus [10]. Since $N=90$ nuclei nearest $Z=64$ are found to be better quantum rotors at low spin [1], it is conceivable that the lack of band termination states in ^{155}Tb suggests that this is still true at high-spin as the $Z=65$ nucleus appears to be more resilient to oblate driving structures.

The $\alpha=+\frac{1}{2}$ signature of the [532]5/2 band begins to gain alignment at very high rotational energy, $\hbar\omega\approx0.57$ MeV, see Fig. 5(b). The $\alpha=-\frac{1}{2}$ signature does not experience any

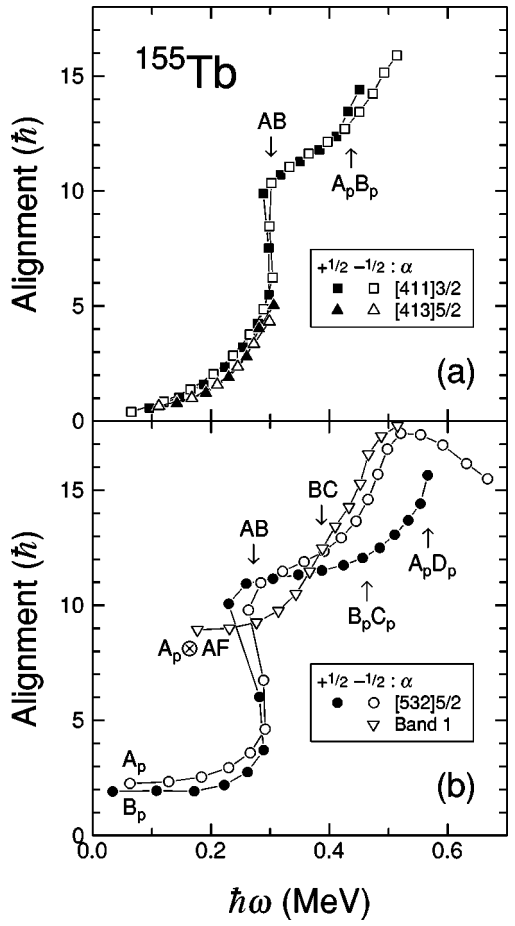

FIG. 5. The rotational alignment of bands observed in ^{155}Tb. The Harris parameters $\mathcal{J}_0=32\hbar^2/\mathrm{MeV}$ and $\mathcal{J}_1=34\hbar^4/\mathrm{MeV}^3$ were used. Bands based on positive-parity orbitals are displayed in panel (a), while bands with a $h_{11/2}$ proton in their initial configuration are shown in panel (b). The solid (open) symbols represent the $\alpha=+\frac{1}{2}(\alpha=-\frac{1}{2})$ signature.

kind of crossing in this frequency region, which implies that this is most likely the A_pD_p crossing. This crossing has only been observed in the $N=90$ isotone ^{161}Lu [27] at $\hbar\omega_c=0.50$ MeV (although the onset of the A_pD_p crossing was indicated in ^{157}Ho [25]). The clear observation of this crossing in ^{155}Tb provides further evidence that proton-pair correlations are still quite significant at very high rotational frequencies ($\hbar\omega\geqslant 0.5$ MeV) and spins ($I\geqslant 35\hbar$) [24].

The large initial alignment of band 1 [Fig. 5(b)] indicates that this band is associated with a three-quasiparticle structure at low frequencies ($\hbar\omega<0.3$ MeV). The band passes through the AB crossing region and appears to gain $\sim 9\hbar$ from one crossing, which is highly unusual except for the AB alignment. Upon further review of Fig. 5(b), one may note the slight change in curvature in the alignment at $\hbar\omega\approx 0.42$ MeV. This kink has been interpreted as being the end of one crossing and the beginning of another. The first crossing occurs at $\hbar\omega_c\approx 0.38$ MeV with a gain of $\Delta i\approx 5\hbar$ and is associated with the alignment of the B and C neutrons. This is consistent with bands found in ^{157}Ho and neighboring even-even nuclei (see Ref. [5] and references therein) where the BC crossings are observed at $\hbar\omega_c\approx 0.37$ MeV with gains of $\Delta i\approx 5\hbar$ in alignment. The second crossing is in the same frequency region ($\hbar\omega_c\approx 0.47$ MeV) as the B_pC_p crossing seen in the $\alpha=-\frac{1}{2}$ signature of the [532]5/2 band. Thus, we attribute the other $\sim 4\hbar$ gain in alignment to this B_pC_p crossing. Two nearby crossings with a total $\Delta i\approx 10\hbar$ are also observed in the $(\pi,\alpha)=(-,0)$ signature of the $\pi h_{11/2}\otimes\nu i_{13/2}$ (AA_p) band in ^{156}Tb [30], which further validates our crossing assignments in band 1.

The existence of the BC crossing in band 1 along with the blocking of the AB crossing strongly suggests that the A neutron is involved initially. In a similar manner, the presence of the B_pC_p crossing and the lack of the gradual gain in alignment of the A_pB_p crossing indicates that the A_p proton is a part of the configuration also. Therefore, only the nature of the other quasineutron is left to determine. We have experimentally determined that band 1 has the signature $\alpha=-\frac{1}{2}$; therefore, the third quasiparticle has $\alpha=-\frac{1}{2}$.[1] As stated

TABLE II. Summary of band crossing frequencies and alignment gains in ^{155}Tb.

Band (π,α), [a] initial configuration	Band crossing	$\hbar\omega_c$ (MeV)	Δi [b] $(\hbar)$
$[411]3/2(+,\pm\frac{1}{2})$, E_p,F_p	AB	0.30(1)	9.8
$[411]3/2(+,\pm\frac{1}{2})$, E_p,F_p	A_pB_p	0.44(2)	$\geqslant 5$
$[532]5/2(-,-\frac{1}{2})$, A_p	AB	0.280(3)	9.3
$[532]5/2(-,-\frac{1}{2})$, A_p	B_pC_p	0.47(1)	5.8
$[532]5/2(-,+\frac{1}{2})$, B_p	AB	0.269(3)	9.3
$[532]5/2(-,+\frac{1}{2})$, B_p	A_pD_p	0.57(2)	>4.5
Band 1 $(+,-\frac{1}{2})$, $A_p\otimes$AF	BC	0.38(1)	~ 5
Band 1 $(+,-\frac{1}{2})$, $A_p\otimes$AF	B_pC_p	0.47(1)	$\geqslant 4$

[a] π and α denote parity and signature, respectively.
[b] Uncertainties in the alignment gains are $\leqslant\pm 1\hbar$.

[1] The signature of a multiquasiparticle band is equal to the sum of the individual quasiparticles involved in its configuration.

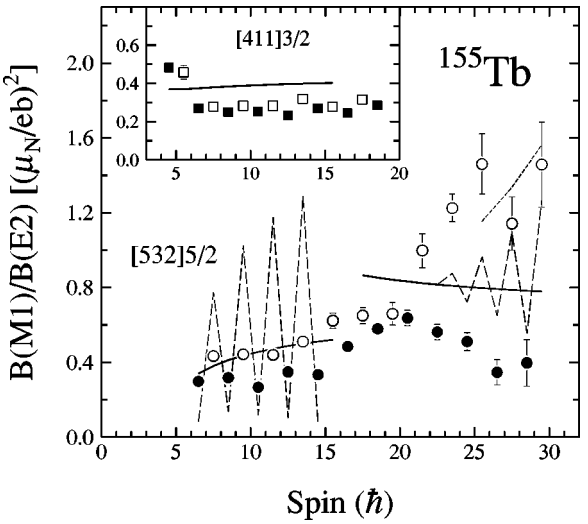

FIG. 6. The experimental (symbols) and theoretical (lines) $B(M1)/B(E2)$ ratios for the [411]3/2 (inset) and [532]5/2 bands in ^{155}Tb. Note that the inset has the same scale as the main plot. The calculations for the [532]5/2 band have excluded (included) the signature splitting term for the solid (dashed) lines. The $\alpha=+\frac{1}{2}$ and $\alpha=-\frac{1}{2}$ signatures are represented by solid and open symbols, respectively.

previously, positive parity has been tentatively given to band 1 due to its similarity with a positive-parity band observed in ^{153}Tb [2]. Thus, the second quasineutron likely originates from a negative-parity neutron orbital near the Fermi surface. Band 1 has, therefore, been assigned as the $A_p \otimes AF$ configuration, which is consistent with the $\sim 7\hbar$ difference in alignment between this band and the [532]5/2 band at low rotational frequency ($\hbar\omega < 0.3$ MeV).

IV. $B(M1)/B(E2)$ TRANSITION STRENGTH RATIOS

Experimental $B(M1)/B(E2)$ ratios were extracted from both experiments using the standard equation

$$\frac{B(M1:I\rightarrow I-1)}{B(E2:I\rightarrow I-2)} = 0.693\frac{E_\gamma^5(I\rightarrow I-2)}{E_\gamma^3(I\rightarrow I-1)}\times\frac{1}{\lambda(1+\delta^2)}\left(\frac{\mu_N}{e\mathrm{b}}\right)^2, \quad (1)$$

where λ is the branching ratio [$\lambda = I_\gamma(I\rightarrow I-2)/I_\gamma(I\rightarrow I-1)$], E_γ is the energy of the γ ray measured in MeV, and δ is the mixing ratio of the $I\rightarrow I-1$ transition. The mixing ratios were determined using branching ratios and assuming pure K with the rotational model [31]. This approach produced values for the [532]5/2 band similar to those measured in the $\pi h_{11/2}$ band of ^{157}Ho [25], and also gave very small ratios for the [411]3/2 band ($\delta \leqslant 0.15$). The experimental $B(M1)/B(E2)$ ratios are plotted in Fig. 6 along with the theoretical predictions.

The theoretical calculations of the $B(M1)/B(E2)$ ratios used the rotational model [31] form of the $B(E2)$ transition strength:

$$B(E2:I\rightarrow I-2) = \frac{5}{16\pi}e^2Q_0^2\langle I2K0|(I-2)K\rangle^2. \quad (2)$$

An intrinsic quadrupole moment of $Q_0 = 6.2$ eb was assumed using the average of the measured quadrupole moments of the neighboring even-even nuclei [32]. The $B(M1)$ transition strengths were determined using an extended formalism [33] of the geometrical model from Dönau [34] and Frauendorf [35]:

$$\begin{aligned} B(M1:I\rightarrow I-1) = \frac{3}{8\pi I^2}\{&\sqrt{I^2-K^2}[(1-\Delta e'/\hbar\omega)(g_{K_1} \\ &- g_R)K_1 + (g_{K_2}-g_R)K_2 + (g_{K_3}-g_R)K_3 + \cdots] \\ &- K[(g_{K_1}-g_R)i_1 + (g_{K_2}-g_R)i_2 + (g_{K_3}-g_R)i_3 \\ &+ \cdots\}^2\mu_N^2 \end{aligned} \quad (3)$$

where $K = K_1 + K_2 + K_3 + \cdots$. The subscripts 1, 2, and 3 refer to the quasiparticles, or aligned pairs of quasiparticles, that couple to form the band, and $\Delta e'$ is the signature splitting of the level energies in the rotating frame. The collective gyromagnetic ratio was determined by $g_R = 0.7(Z/A)$, while the g_K values were calculated using a Woods-Saxon potential [36] (the standard $g_K = -0.20$ was used for the $i_{13/2}$ neutrons). The initial alignments (i_1) were obtained from Fig. 5 at low rotational frequency ($\hbar\omega = 0.1$ MeV) and the alignments of the quasiparticle pairs (i_2, i_3) are equal to the alignment gain Δi of the given crossing as reported in Table II. The parameters used in the theoretical calculations of the $B(M1)/B(E2)$ ratios are summarized in Table III where the subscript 1 represents the initial quasiproton, 2 represents the AB quasineutrons, and 3 the B_pC_p quasiprotons.

The experimental $B(M1)/B(E2)$ ratios for the [411]3/2 band, shown in the inset of Fig. 6, are quite consistent at $\sim 0.3(\mu_N/e\mathrm{b})^2$. The theoretical prediction overestimates the ratios: this is likely due to mixing between the pseudo-spin partner [411]3/2 and [413]5/2 bands. A rise in the ratios would be expected above $I = \frac{33}{2}$ because of the alignment of the $i_{13/2}$ neutrons. However, with only a few $\Delta I = 1$ transitions observed in the band crossing region, our expectations cannot be confirmed.

One can observe the experimental signature dependence of the $B(M1)/B(E2)$ ratios in the one-quasiparticle region, $I < \frac{33}{2}$, of the [532]5/2 band (see Fig. 6). An attempt to reproduce this effect using the signature splitting term ($\Delta e'$) of Eq. (3) is displayed in Fig. 6 as the low-spin dashed line. An overestimation of the splitting by an order of magnitude is observed. This deficiency is similar to that reported for the

TABLE III. Parameters used in the calculation of $B(M1)/B(E2)$ ratios.

Band	$Q_0(e$ b)	g_R	g_{K_1}	$K_1(\hbar)$	$i_1(\hbar)$	g_{K_2}	$K_2(\hbar)$	$i_2(\hbar)$	g_{K_3}	$K_3(\hbar)$	$i_3(\hbar)$
[411]3/2	6.2	0.29	1.81	1.5	1.1	−0.20	0	9.8			
[532]5/2	6.2	0.29	1.43	2.5	2.5	−0.20	0	9.3	1.43	1	5.8

$\pi h_{11/2}$ band in ^{157}Ho [25]. Equation (3) assumes an axially symmetric shape; therefore, other suggestions have introduced γ deformation or γ-vibration effects from the $\pi h_{11/2}$ bands as possible causes for the splitting. More discussion of this phenomenon follows in the next section. The theoretical calculations shown in Fig. 6 as solid lines have $\Delta e' = 0$ MeV and a general agreement can be seen between theory and experiment in the one-quasiparticle region.

In the spin region $\frac{31}{2} \leqslant I \leqslant \frac{43}{2}$, the $B(M1)/B(E2)$ ratios begin to increase and the values for both signatures become similar. This is due to the alignment of the $i_{13/2}$ neutrons as indicated by the theoretical ratios (solid line at high-spin). Above spin $I = \frac{43}{2}$, significant signature dependence arises once more. Since the $i_{13/2}$ neutrons are predicted to polarize the nucleus towards a symmetric prolate shape, the geometrical model should be able to reproduce the observed splitting. The $\Delta e'$ term of Eq. (3) was used again in the calculation of the dashed line at high spin. While initially the model underestimates the splitting, the data are nearly reproduced by the calculations at the highest observed spins. The splitting may be caused by the onset of the B_pC_p crossing; therefore, these quasiprotons were accounted for in the calculation of the $\alpha = -\frac{1}{2}$ signature at high-spin (short dashed line above $I = \frac{51}{2}$). Again a reasonable agreement is achieved between theory and experiment for this signature.

V. SIGNATURE SPLITTING OF THE $\pi h_{11/2}$ BANDS IN ODD-$A \approx 160$ NUCLEI

A strong signature dependence on the levels of the [523]7/2 band in ^{159}Tm was first brought to attention by Larabee and Waddington [37]. This result was quite surprising as one would expect both signatures to be almost equally energetically favored given the high-K nature of this band. Similar discoveries were found in the unique-parity bands of ^{155,157}Ho and ^{161,163,165}Lu. The signature dependence was not only observed in the energy levels where the $\alpha = -\frac{1}{2}$ signature is favored, but also occured in the $B(M1)/B(E2)$ ratios where larger values were found in the $\alpha = -\frac{1}{2}$ signature. While the signature splitting in the levels could possibly be explained by unusually large mixing from the $K = \frac{1}{2}$ orbital, the amount of $B(M1)/B(E2)$ splitting could not be accounted for by simple mixing. Instead, various theoretical studies, using different models (e.g., the particle rotor model [38–49] or the cranked shell model [45,50–53]) have proposed that the $h_{11/2}$ quasiprotons drive the nucleus to stable γ mdeformed (triaxial) shapes or vibrate between symmetric and triaxial shapes, which could describe both the energy and $B(M1)/B(E2)$ ratio splitting before the AB crossing.

A significant amount of experimental work has been performed on the odd-$A \approx 160$ nuclei since the aforementioned theoretical studies were conducted. The signature splitting of the energy levels and $B(M1)/B(E2)$ ratios are displayed for these nuclei in Figs. 7 and 8, respectively. For discussion purposes, the calculated quadrupole deformation (β_2) of each nucleus from Ref. [54] has also been given in Fig. 7. The large region of deformation covered by these nuclei and the occupation of nearly every orbital in the $h_{11/2}$ shell (from $K = \frac{1}{2}$ or $\frac{3}{2}$ in ^{151}Eu and ^{153}Tb to $K = \frac{9}{2}$ in ^{161,163,165}Lu) will reveal the dependence that the signature splitting phenomenon has on β_2 and the proton Fermi surface λ. Data for the nuclei, other than ^{155}Tb, were compiled from the following sources: ^{151}Eu [55,56], ^{153}Eu [57], ^{155}Eu [3], ^{153}Tb [2], ^{157}Tb [3], ^{155}Ho [58], ^{157}Ho [25], ^{159}Ho [59,60], ^{161}Ho [61], ^{157}Tm [62], ^{159}Tm [26], ^{161}Tm [63], ^{163}Tm [64], ^{159}Lu [65], ^{161}Lu [27], ^{163}Lu [28], ^{165}Lu [66].

A. Experimental observations and possible interpretations in the low-spin region $I < \frac{33}{2}$

(1) The $N = 88$ nuclei all have very large and consistent energy splitting before the AB crossing. These nuclei are still under the influence of the $Z = 64$ shell gap, which may be partially responsible for the observed splitting. Since the $h_{11/2}$ shell lies higher in energy in the $N = 88$ nuclei compared with the $N \geqslant 90$ nuclei [1], the proton Fermi level λ will lie closer to the low-K components of the shell. Therefore, large energy splitting would indeed be expected from bands containing a substantial $K = \frac{1}{2}$ component in their wave-functions. Cranked shell model calculations [50] suggest that the low-K orbitals do not drive towards large γ values, which raises the question of whether triaxial deformation or normal Coriolis coupling is predominantly causing the energy splitting. Perhaps γ deformation is more important in ^{157}Tm and ^{159}Lu where λ is likely to be near the mid-K values and the quadrupole deformations are quite weak. Unfortunately, since the energy splitting is so large, the $\Delta I = 1$, $\alpha = -\frac{1}{2} \rightarrow \alpha = +\frac{1}{2}$ transitions have not been observed and thus, no clues can be extracted from the $B(M1)/B(E2)$ ratios (see Fig. 8).

(2) A reduction in the energy and $B(M1)/B(E2)$ ratio splitting is observed as the neutron number is increased. This is most likely a function of the quadrupole deformation β_2 increasing with increasing neutron number (see Fig. 7). The larger β_2 values suggest that the nuclei are better rotors, and are thus more resistant to the polarization effects of the γ driving $h_{11/2}$ protons. The Fermi surface moves further away from the $K = \frac{1}{2}$ orbital as the quadrupole deformation increases, which would also decrease the amount of splitting observed.

(3) As Z decreases in the $N \geqslant 90$, Ho, Tm, and Lu nuclei, the splitting decreases. Similar to trend (2), this is likely due to the increasing β_2 deformation as Z decreases in these three nuclei (see Fig. 7). However, as suggested by the calculations in Ref. [50], the lowering of the Fermi surface in the $h_{11/2}$ shell would also cause a reduction in the γ driving force of the quasiprotons and thus may contribute to the diminished splitting.

(4) A particularly interesting region of Figs. 7 and 8 is that of the $N = 90$ and 92 Eu, Tb, and Ho nuclei. There the quadrupole deformation is essentially constant; therefore, other variables must be considered as the leading cause(s) for any change in the splitting as a function of Z. As one can observe in Fig. 7, the energy splitting increases as Z decreases from Ho to Tb, and then remains nearly constant as Z decreases again from Tb to Eu. However, the $B(M1)/B(E2)$ ratios (see Fig. 8) exhibit less splitting as Z decreases. The transition strength ratios are consistent with the scenario that the γ driving tendencies wane as the Fermi surface is lowered. By moving the Fermi level λ from near the $K = \frac{7}{2}$ orbital in Ho to $K = \frac{5}{2}$ in Eu and Tb, the influence of the K

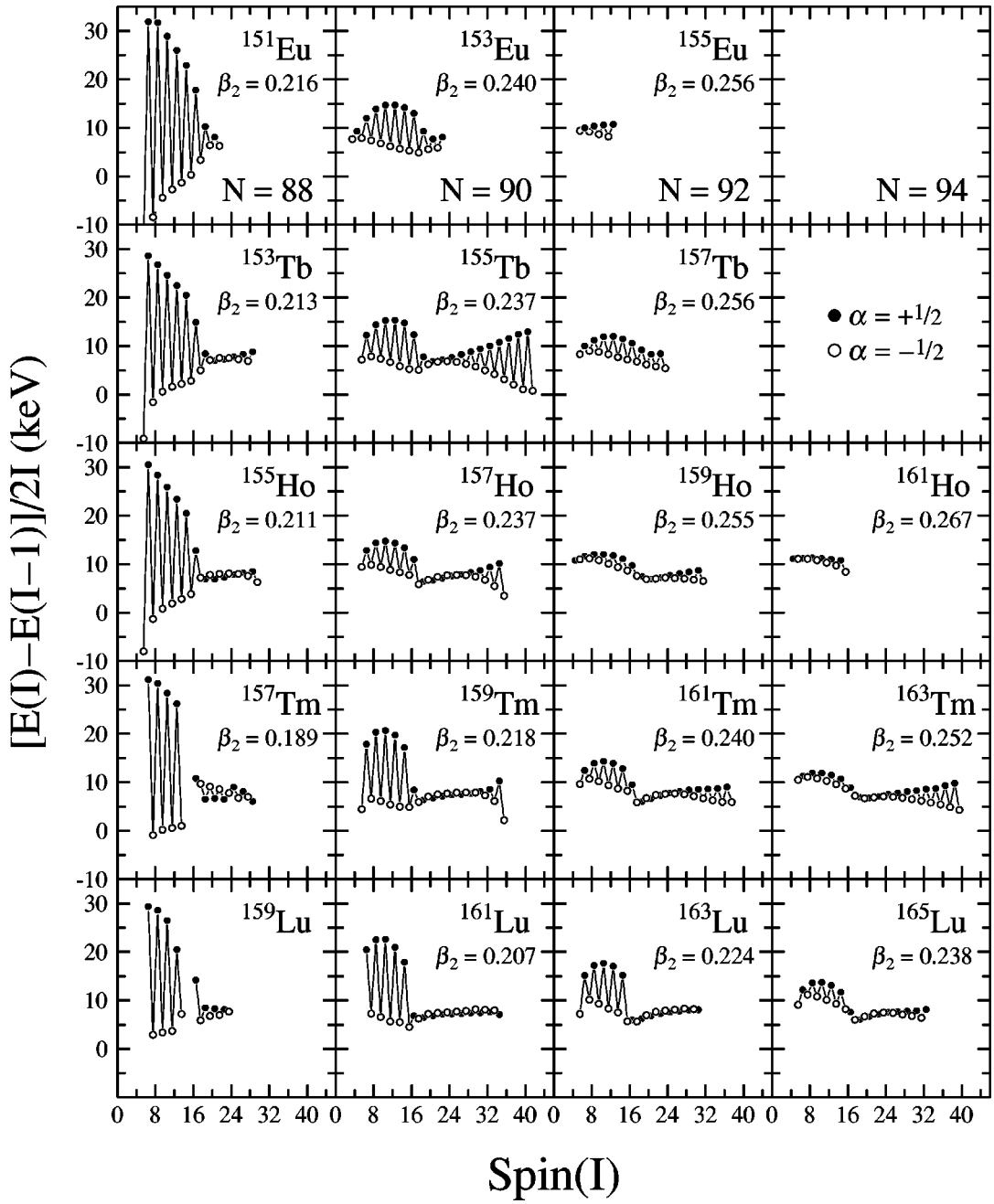

FIG. 7. Energy level splitting of the $\pi h_{11/2}$ bands in the $A \approx 160$ region. The $\alpha = +\frac{1}{2}$ and $\alpha = -\frac{1}{2}$ signatures are represented by solid and open symbols, respectively. References used are given in the text.

$=\frac{1}{2}$ orbital may be more responsible for the increased energy splitting.

B. Experimental observations and possible interpretations of the high-spin region $I > \frac{33}{2}$

(1) A quenching of the energy and, in general, of the $B(M1)/B(E2)$ splitting occurs with the alignment of the lowest pair of $i_{13/2}$ neutrons. It has been suggested that these high-j neutrons polarize the nuclear shape back to near prolate symmetric shapes, thus essentially eliminating the splitting [51,52]. This idea is supported by noting that the $\pi h_{11/2} \otimes \nu i_{13/2}$ bands in neighboring odd-odd nuclei have comparatively small energy splitting [67]. However, not only is the splitting reduced for the bands shown in Figs. 7 and 8, but for ^{153}Tb, ^{155,157}Ho, ^{157,159,161}Tm, and ^{161,163,165}Lu the normally unfavored $\alpha = +\frac{1}{2}$ signature even becomes slightly favored. While some conjectures have been made (e.g., the $i_{13/2}$ neutrons drive towards slightly positive γ values [52] or the interaction of particle-γ vibration coupling [43]), more theoretical work is needed to fully understand this inversion process.

(2) A change back to the normal energy splitting is observed in many of the nuclei where signature inversion occurred. These reversions begin at various spin values (see Fig. 7) and may be caused by different conditions. The band terminating states above $I = \frac{57}{2}$ [62] in the $N = 88$ nuclei may interfere with the inversion process for these nuclei. The B_pC_p crossing is the cause of the reversion in the $N = 90$

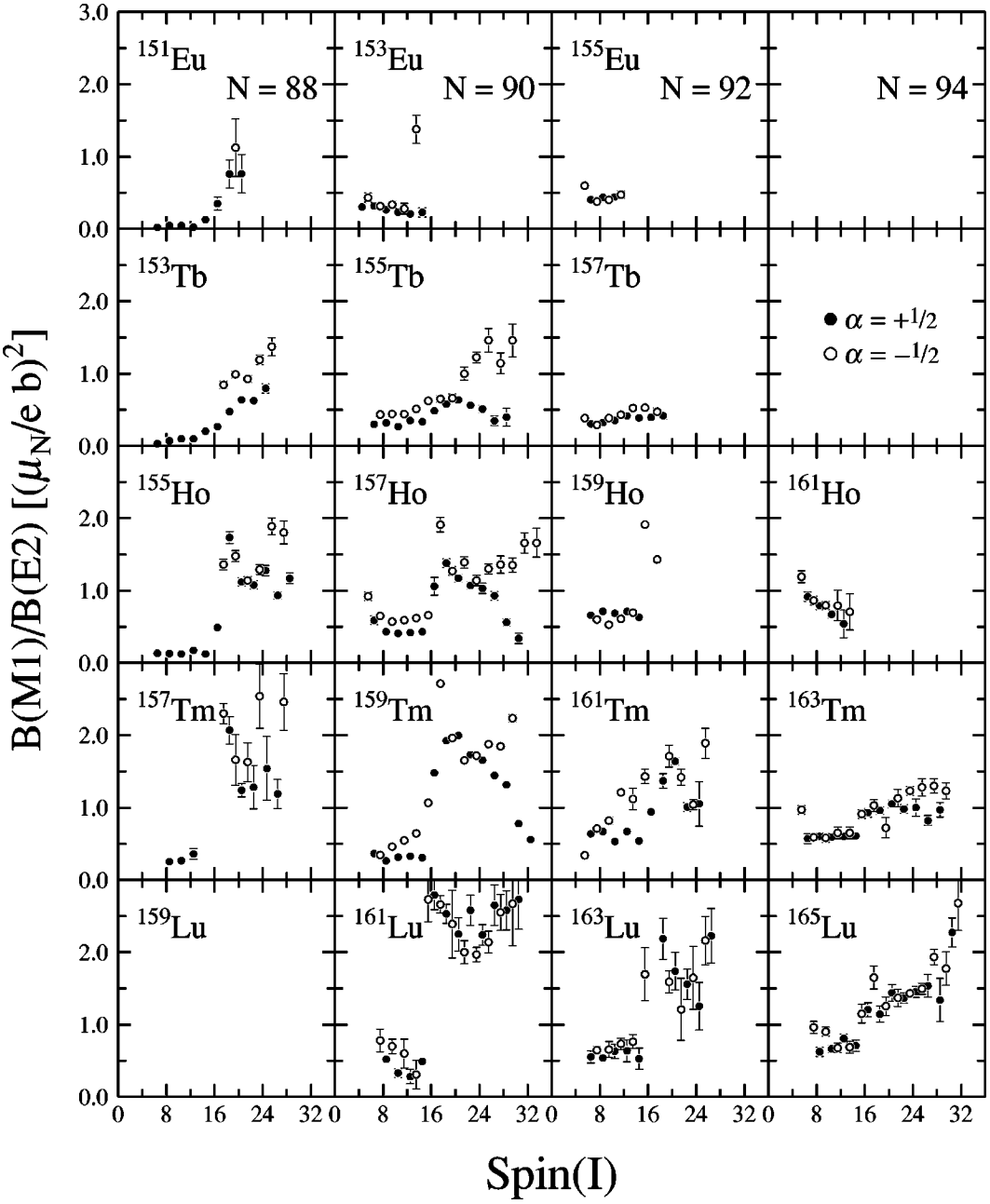

FIG. 8. $B(M1)/B(E2)$ ratios of the $\pi h_{11/2}$ bands in the $A \approx 160$ region. The $\alpha = +\frac{1}{2}$ and $\alpha = -\frac{1}{2}$ signatures are represented by solid and open symbols, respectively. References used are given in the text.

nuclei as the alignment compresses the states in the $\alpha = -\frac{1}{2}$ signature such that they become energetically favored over the $\alpha = +\frac{1}{2}$ signature. Although this crossing occurs at approximately the same frequency ($\hbar\omega_c \approx 0.47$ MeV) in ^{155}Tb, ^{157}Ho, and ^{159}Tm, the reversion begins at different spins in each nucleus. The variation of the interaction strength V_ω for the B_pC_p crossing in these nuclei most likely produces this difference. A weak interaction strength is observed in ^{159}Tm, while ^{157}Ho has a stronger V_ω, and ^{155}Tb has the strongest of the three. The crossing is stretched over a larger spin region with increasing V_ω; thus, the lighter nuclei return to normal and larger signature splitting quicker. In ^{161}Lu, this proton crossing is not observed and thus, a reversion to normal ordering is also missing. The return to large splitting is also observed in the $B(M1)/B(E2)$ ratios at very high-spin for ^{155}Tb, ^{157}Ho, and ^{159}Tm (see Fig. 8). As shown in Sec. IV A, this may be the result of the B_pC_p crossing in a symmetric nucleus. It is not so evident what causes the reversion in the heavier ^{161,163}Tm and ^{165}Lu nuclei at this time; however, a common factor in these nuclei is that they all experience the CD crossing at very high spin.

The experimental systematics of the signature splitting phenomenon are now essentially complete (although precise lifetime measurements would still be desirable for the majority of the bands). However, a consistent theoretical picture for both the low-spin and high-spin regions has not yet fully emerged. The possiblity of signature dependent shapes, the signature inversion problem, the variation and variety of ro-

tational alignments, incorporating the $Z=64$ subshell gap for the $N=88$ nuclei, and other effects make this a particularly challenging puzzle.

VI. SUMMARY

The combination of our two experiments has added over 115 new transitions to the level scheme of ^{155}Tb with the extensions of three bands to very high-spin ($I \leqslant \frac{95}{2}$). One new decoupled structure was observed and its configuration has been assigned through the measured alignment profile. Various quasiparticle band crossings were identified and found to be consistent with those observed in other nearby nuclei. While the $\alpha=-\frac{1}{2}$ signature of the [532]5/2 band was extended into the spin region where band termination effects have been seen in many $N=90$, no evidence for such structures was found in ^{155}Tb. General agreement was found between experimental and theoretical $B(M1)/B(E2)$ ratios for the [411]3/2 and [532]5/2 bands. The experimental trends in the signature splitting of the $h_{11/2}$ bands for $A \approx 160$ nuclei were investigated. The latter splitting apparently has (among other possible quantities) a large dependence on the quadrupole deformation (β_2) and the placement of the proton Fermi surface (λ). More work is still needed to unravel the full systematic behavior of signature splitting and signature inversion in this wide range of odd-Z, odd-A nuclei.

ACKNOWLEDGMENTS

Special thanks to D. C. Radford and H. Q. Jin for their software support and also to R. Darlington for help with the targets. Support for this work was provided by the U.S. Department of Energy, Nuclear Physics Division, under Contract Nos. W-31-109-ENG-38 (ANL) and DE-FG05-95ER40939 (MSU), and by the National Science Foundation and the State of Florida (FSU). M.A.R. and J.S. acknowledge the receipt of a NATO Collaborative Research Grant.

[1] R. F. Casten, D. D. Warner, D. S. Brenner, and R. L. Gill, Phys. Rev. Lett. **47**, 1433 (1981).
[2] D. J. Hartley, T. B. Brown, F. G. Kondev, R. W. Laird, J. Pfohl, A. M. Richmond, M. A. Riley, J. Döring, and J. Simpson, Phys. Rev. C **58**, 1321 (1998).
[3] D. J. Hartley, M. A. Riley, D. E. Archer, T. B. Brown, J. Döring, R. A. Kaye, F. G. Kondev, T. Petters, J. Pfohl, R. K. Sheline, J. Simpson, and S. L. Tabor, Phys. Rev. C **57**, 2944 (1998).
[4] S. L. Tabor, M. A. Riley, J. Döring, P. D. Cottle, R. Books, T. Glasmacher, J. W. Holcomb, J. Hutchins, G. D. Johns, T. D. Johnson, T. Petters, O. Tekyi-Mensah, P. C. Womble, L. Wright, and J. X. Saladin, Nucl. Instrum. Methods Phys. Res. B **79**, 821 (1993).
[5] J. D. Morrison, J. Simpson, M. A. Riley, H. W. Cranmer-Gordon, P. D. Forsyth, D. Howe, and J. F. Sharpey-Schafer, J. Phys. G **15**, 1871 (1989).
[6] D. C. Radford, Nucl. Instrum. Methods Phys. Res. A **361**, 297 (1995).
[7] ''GAMMASPHERE, A National Gamma-ray Facility,'' edited by M. A. Deleplanque and R. M. Diamond, Lawrence Berkeley Laboratory, Berkeley, Report No. PUB-5202, 1988; I. Y. Lee, Nucl. Phys. **A520**, 641c (1990).
[8] P. J. Nolan, F. A. Beck, and D. B. Fossan, Annu. Rev. Nucl. Part. Sci. **45**, 561 (1994).
[9] C. W. Beausang and J. Simpson, J. Phys. G **22**, 527 (1996).
[10] F. G. Kondev, M. A. Riley, R. V. F. Janssens, J. Simpson, A. V. Afanasjev, I. Ragnarsson, I. Ahmad, D. J. Blumenthal, T. B. Brown, M. P. Carpenter, P. Fallon, S. M. Fischer, G. Hackman, D. J. Hartley, C. A. Kalfas, T. L. Khoo, T. Lauritsen, W. C. Ma, D. Nisius, J. F. Sharpey-Schafer, and P. G. Varmette, Phys. Lett. B (in press).
[11] T. B. Brown *et al.* (unpublished).
[12] W. C. Ma *et al.* (unpublished).
[13] G. Winter, L. Funke, K.-H. Kaun, P. Kemnitz, and H. Sodan, Nucl. Phys. **A176**, 609 (1971).
[14] J. C. Tippett and D. G. Burke, Can. J. Phys. **50**, 3152 (1972).
[15] M. A. Riley, D. J. Hartley, J. Simpson, J. F. Sharper-Schafer, D. E. Archer, T. B. Brown, J. Döring, P. Fallon, C. A. Kalfas, and S. L. Tabor, Phys. Rev. C **53**, 989 (1996).
[16] B. A. Alikov, Kh. N. Badalov, V. O. Nesterenko, A. V. Sushkov, and J. Wawryszczuk, Z. Phys. A **331**, 265 (1988).
[17] D. Nosek, R. K. Sheline, P. C. Sood, and J. Kvasil, Z. Phys. A **344**, 277 (1993).
[18] A. V. Afanasjev and I. Ragnarsson, Phys. Rev. C **51**, 1259 (1995).
[19] S. M. Harris, Phys. Rev. B **138**, B509 (1965).
[20] R. Bengtsson and S. Frauendorf, Nucl. Phys. **A314**, 27 (1979); **A327**, 139 (1979).
[21] L. L. Riedinger, O. Anderson, S. Frauendorf, J. D. Garrett, J. J. Gaardhøje, G. B. Hagemann, B. Herskind, Y. V. Makovetzky, J. C. Waddington, M. Guttormsen, and P. O. Tjøm; Phys. Rev. Lett. **44**, 568 (1980).
[22] R. Bengtsson, S. Frauendorf, and F.-R. May, At. Data Nucl. Data Tables **35**, 15 (1986).
[23] M. A. Riley, J. Simpson, J. F. Sharpey-Schafer, J. R. Cresswell, H. W. Cranmer-Gordon, P. D. Forsyth, D. Howe, A. H. Nelson, P. J. Nolan, P. J. Smith, N. J. Ward, J. C. Lisle, E. Paul, and P. M. Walker, Nucl. Phys. **A486**, 456 (1988).
[24] J. Simpsonw, P. D. Forsyth, D. Howe, B. M. Nyakó, M. A. Riley, J. F. Sharpey-Schafer, J. Bacelar, J. D. Garrett, G. B. Hagemann, B. Herskind, A. Holm, and P. O. Tjøm, Phys. Rev. Lett. **54**, 1132 (1985).
[25] D. C. Radford, H. R. Andrews, G. C. Ball, D. Horn, D. Ward, F. Banville, S. Flibotte, S. Monaro, S. Pilotte, P. Taras, J. K. Johansson, D. Tucker, J. C. Waddington, M. A. Riley, G. B. Hagemann, and I. Hamamoto, Nucl. Phys. **A545**, 665 (1992).
[26] D. C. Radford (private communication).
[27] C.-H. Yu, M. A. Riley, J. D. Garrett, G. B. Hagemann, J. Simpson, P. D. Forsyth, A. R. Mokhtar, J. D. Morrison, B. M. Nyakó, and R. Wyss, Nucl. Phys. **A489**, 477 (1988).
[28] W. Schmitz, C. X. Yang, H. Hübel, A. P. Byrne, R. Müsseler, N. Singh, K. H. Maier, A. Kuhnert, and R. Wyss, Nucl. Phys. **A539**, 112 (1992).

[29] R. D. Ratna Raju, J. P. Draayer, and K. T. Hecht, Nucl. Phys. **A202**, 433 (1973).
[30] D.J. Hartley *et al.* (unpublished).
[31] A. Bohr and B.R. Mottelson, *Nuclear Structure* (Benjamin, New York, 1975), Vol. 2.
[32] S. Raman, C. H. Malarkey, W. T. Milner, C. W. Nestor, Jr., and P. H. Stelson, At. Data Nucl. Data Tables **36**, 1 (1987).
[33] V. P. Janzen, Z.-M. Liu, M. P. Carpenter, L. H. Courtney, H.-Q. Jin, A. J. Larabee, L. L. Riedinger, J. K. Johansson, D. G. Popescu, J. C. Waddington, S. Monaro, S. Pilotte, and F. Dönau, Phys. Rev. C **45**, 613 (1992).
[34] F. Dönau, Nucl. Phys. **A471**, 469 (1987).
[35] S. Frauendorf, Phys. Lett. **100B**, 219 (1981).
[36] S. Ćwiok, J. Dudek, W. Nazarewicz, J. Skalski, and T. Werner, Comput. Phys. Commun. **46**, 379 (1987); J. Dudek, A. Majhofer, J. Skalski, T. Werner, S. Ćwiok, and W. Nazarewicz, J. Phys. G **5**, 1359 (1979).
[37] A. J. Larabee and J. C. Waddington, Phys. Rev. C **24**, 2367 (1981).
[38] A. Ikeda, Nucl. Phys. **A439**, 317 (1985).
[39] I. Hamamoto and B. Mottelson, Phys. Lett. **167B**, 370 (1986).
[40] I. Hamamoto, Phys. Lett. B **179**, 327 (1986).
[41] A. Ikeda and S. Åberg, Nucl. Phys. **A480**, 85 (1988).
[42] I. Hamamoto and H. Sagawa, Phys. Lett. B **201**, 415 (1988).
[43] A. Ikeda and T. Shimano, Phys. Rev. Lett. **63**, 139 (1989).
[44] M. Matsuzaki, Nucl. Phys. **A491**, 433 (1989).
[45] G. B. Hagemann and I. Hamamoto, Phys. Rev. C **40**, 2862 (1989).
[46] A. Ikeda and T. Shimano, Phys. Rev. C **42**, 149 (1990).
[47] I. Hamamoto, Nucl. Phys. **A520**, 297c (1990).
[48] N. Tajima, Nucl. Phys. **A520**, 317c (1990).
[49] T. Mathur and N. Mukherjee, Phys. Rev. C **49**, 142 (1994).
[50] G. A. Leander, S. Frauendorf, and F. R. May, *Proceedings of the Conference on High Angular Momentum Properties of Nuclei*, edited by N. R. Johnson (Harwood, New York, 1983), p. 281.
[51] S. Frauendorf and F. R. May, Phys. Lett. **125B**, 245 (1983).
[52] Y. S. Chen, S. Frauendorf, and L. L. Riedinger, Phys. Lett. B **171**, 7 (1986).
[53] M. Matsuzaki, Nucl. Phys. **A504**, 456 (1989).
[54] W. Nazarewicz, M. A. Riley, and J. D. Garrett, Nucl. Phys. **A512**, 61 (1990).
[55] W. J. Vermeer, W. Urban, M. K. Khan, C. J. Pearson, A. B. Wiseman, B. J. Varley, J. L. Durell, and W. R. Phillips, Nucl. Phys. **A559**, 422 (1993).
[56] J. R. Jongman, W. Urban, J. C. S. Bacelar, J. van Pol, J. Nyberg, G. Sletten, J. S. Dionisio, Ch. Vieu, J. M. Lagrange, and M. Pautrat, Nucl. Phys. **A591**, 244 (1995).
[57] C. J. Pearson, W. R. Phillips, J. L. Durell, B. J. Varley, W. J. Vermeer, W. Urban, and M. K. Khan, Phys. Rev. C **49**, R1239 (1994).
[58] J. Simpson (private communication).
[59] I. Forsblom, S. A. Hjorth, and A. Špalek, Nucl. Phys. **A252**, 315 (1975).
[60] C.-H. Yu (private communication).
[61] L. Funke, K.-H. Kaun, P. Kemnitz, H. Sodan, and G. Winter, Nucl. Phys. **A170**, 593 (1971).
[62] M. A. Riley, T. B. Brown, N. R. Johnson, Y. A. Akovali, C. Baktash, M. L. Halbert, D. C. Hensley, I. Y. Lee, F. K. McGowan, A. Virtanen, M. E. Whitley, J. Simpson, L. Chaturvedi, L. H. Courtney, V. P. Janzen, L. L. Riedinger, and T. Bengtsson, Phys. Rev. C **51**, 1234 (1995).
[63] A. G. Smith, R. Chapman, D. C. Clarke, J. Copnell, S. J. Freeman, F. Khazaie, G. S. Li, J. C. Lisle, J. N. Mo, C. Tenreiro, D. M. Thompson, G. J. Yuan, J. Espino, and G. B. Hagemann, Nucl. Phys. **A587**, 150 (1995).
[64] H. J. Jensen, G. B. Hagemann, P. O. Tjøm, S. Frauendorf, A. Atac, M. Bergström, A. Bracco, A. Brockstedt, H. Carlsson, P. Ekström, J. M. Espino, B. Herskind, F. Ingebretsen, J. Jongman, S. Leoni, R. M. Lieder, T. Lönnroth, A. Maj, B. Million, A. Nordlund, J. Nyberg, M. Piiparinen, H. Ryde, M. Sugawara, and A. Virtanen, Z. Phys. A **340**, 351 (1991); H. J. Jensen (private communication).
[65] Y. Ma, H. Sun, Y. Liu, S. Wen, H. Zheng, S. Li, G. Li, G. Yuan, P. Weng, and C. Yang, J. Phys. G **21**, 937 (1995).
[66] P. Frandsen, R. Chapman, J. D. Garrett, G. B. Hagemann, B. Herskind, C.-H. Yu, K. Schiffer, D. Clarke, F. Khazaie, J. C. Lisle, J. N. Mo, L. Carlén, P. Ekström, and H. Ryde, Nucl. Phys. **A489**, 508 (1988); P. Frandsen, J. D. Garrett, G. B. Hagemann, B. Herskind, M. A. Riley, R. Chapman, J. C. Lisle, J. N. Mo, L. Carlen, J. Lyttkens, H. Ryde, and P. M. Walker, Phys. Lett. B **177**, 287 (1986).
[67] M. A. Cardona, M. E. Debray, D. Hojman, A. J. Kreiner, H. Somacal, J. Davidson, M. Davidson, D. De Acuña, D. R. Napoli, J. Rico, D. Bazzacco, R. Burch, S. M. Lenzi, C. Rossi Alvarez, N. Blasi, and G. Lo Bianco, Z. Phys. A **354**, 5 (1996).